Temporal and spatial analysis of ozone concentrations in Europe based on time scale decomposition and a multi-clustering approach

Eirini Boleti[1,2], Christoph Hueglin[1], Stuart K. Grange[1,4], André S. H. Prévôt[3], and Satoshi Takahama[2]

[1]Empa, Swiss Federal Laboratories for Materials Science and Technology, Überlandstrasse 129, Dübendorf, Switzerland
[2]EPFL,École Polytechnique Fédérale de Lausanne, Route Cantonale, 1015 Lausanne, Switzerland
[3]PSI, Paul Scherrer Institute, 5232 Villigen, Switzerland
[4]Wolfson Atmospheric Chemistry Laboratories, University of York, York, YO10 5DD, UK

Correspondence to: Christoph Hueglin (Christoph.Hueglin@empa.ch)

Abstract.

Air quality measures that were implemented in Europe in the 1990s resulted in reductions of ozone precursors concentrations. In this study, the effect of these reductions on ozone is investigated by analyzing surface measurements of this pollutant for the time period between 2000 and 2015. Using a non-parametric time scale decomposition methodology, the long-term, seasonal and short-term variation of ozone observations were extracted. A clustering algorithm was applied to the different time scale variations, leading to a classification of sites across Europe based on the temporal characteristics of ozone. The clustering based on the long-term variation resulted in a site type classification, while a regional classification was obtained based on the seasonal and short-term variations. Long-term trends of de-seasonalized mean and meteo-adjusted peak ozone concentrations were calculated across large parts of Europe for the time period 2000-2015. A multi-dimensional scheme was used for a detailed trend analysis, based on the identified clusters, which reflect precursor emissions and meteorological influence either on the inter-annual or the short-term time scale. Decreasing mean ozone concentrations at rural sites and increasing or stabilizing at urban sites were observed. At the same time downward trends for peak ozone concentrations were detected for all site types. In addition, a reduction of the amplitude in the seasonal cycle of ozone was observed, and a shift in the occurrence of the seasonal maximum towards earlier time of the year. Finally, a reduced sensitivity of ozone to temperature was identified. It was concluded that long-term trends of mean and peak ozone concentrations are mostly controlled by precursors emissions changes, while seasonal cycle trends and changes in the sensitivity of ozone to temperature are among other factors driven by regional climatic conditions.

1 Introduction

Tropospheric ozone (O_3), together with particulate matter and nitrogen dioxide (NO_2), is one of the most troublesome air pollutants in Europe (EEA, 2016). 17,000 premature deaths every year are attributed to excess O_3 exposure, without any sign of reduction in number of fatalities (EEA, 2016). In terms of impact on ecosystems, elevated concentrations of tropospheric O_3 are responsible for damaging agricultural production and forests mainly by reducing their growth rate. In addition, tropospheric O_3 acts as a greenhouse gas with an estimated globally averaged radiative forcing of $0.4\pm0.2\,W/m^2$ (IPCC, 2013). In the

1990s emission control measures on O_3 precursors, namely nitrogen oxides (NO_x=NO+NO_2) and volatile organic compounds (VOCs), were implemented in order to regulate air pollution. As a result, concentrations of NO_x and VOCs have significantly declined in Europe (EEA, 2017; Colette et al., 2011; Guerreiro et al., 2014; Henschel et al., 2015). Especially, NO_x emissions declined in Europe by 48% between 1990 and 2015 (EEA, 2017).

5   Surprisingly, O_3 concentrations have not decreased as was expected (Oltmans et al., 2013; Colette et al., 2018). Mean O_3 concentrations have either remained stable or even increased in rural, background areas from 1990s and until mid-2000s in many European countries (Boleti et al., 2018; Munir et al., 2013; Paoletti et al., 2014; Querol et al., 2016; Anttila and Tuovinen, 2009, e.g.). At urban sites an increase of mean O_3 has been observed; in some cases, an increase has been found at both rural and urban sites with larger upward trends observed at urban compared to the rural sites (Paoletti et al., 2014; Querol

10   et al., 2016; Anttila and Tuovinen, 2009). However, a change in the trend has been observed after mid-2000s, when mean O_3 concentrations have started to decline (Boleti et al., 2018; Munir et al., 2013). On the other hand, maximum O_3 concentrations decreased continuously from the 1990s until present (Paoletti et al., 2014), except for the traffic loaded environments (Boleti et al., 2019). Downward trends of different metrics for peak O_3 have been found at many sites across Europe (Fleming et al., 2018). However, the high year to year variability of O_3 tends to mask the long-term changes leading to a large fraction of sites

15   with non-significant trends . Several studies based on either observations or climate models have shown that anthropogenic emissions can affect O_3 concentrations across continents (Dentener et al., 2010; Wild and Akimoto, 2001; Lin et al., 2017). The increase of background O_3 in Europe has been associated with increasing stratospheric O_3 contribution (Ordóñez et al., 2007), as well as increased hemispheric transport of O_3 and its precursors.

A shift in the seasonal cycle of O_3 has been observed in northern mid-latitudes, i.e. the peak concentrations are now observed
20   earlier in the year compared to previous decades with a rate of 3-6 days/decade. (Parrish et al., 2013). This shift is attributed to increasing emissions of O_3 precursors in developing countries, that led to an equatorward redistribution of precursors in the previous decades (Zhang et al., 2016). Negative trends of the 95th percentile of O_3 and positive trends for the 5th percentile have been detected across Europe (Yan et al., 2018). Simultaneous decrease of maximum concentrations in summer and increase in winter indicate a decrease of amplitude in the seasonal variation of O_3, probably as a result of the regulations in the 1990s
25   (Simon et al., 2015).

O_3 variations are largely governed by climate and weather variability (Yan et al., 2018). Especially temperature influences O_3 concentrations in the troposphere, mainly by increasing the rates of several chemical reactions, and by increasing emissions of biogenic VOCs with increasing temperature (Sillman and Samson, 1995). Thermal decomposition of peroxyacyl nitrates (PANs) at high air temperature conditions results in elevated O_3 concentrations (Dawson et al., 2007). Indeed, extreme O_3 con-
30   centrations in central Europe are mainly associated with high temperatures (Otero et al., 2016). However, there are indications that the relationship of O_3 to temperature has changed in the last 20 years. For instance, in the U.S., O_3 climate penalty – defined as the slope of the O_3 versus temperature relationship – dropped from 3.2 ppbv/°C before 2002 to 2.2 ppbv/°C after 2002 as a result of NO_x emission reductions (Bloomer et al., 2009). Additionally, Colette et al. (2015), based on chemistry-transport and climate-chemistry model projections, assessed the impact of climate change on the climate penalty and found that over

European land surfaces summer O$_3$ change is [0.44; 0.64] and [0.99; 1.50] ppbv (95% confidence interval) for the 2041-2070 and 2071-2100 time periods, respectively.

At different locations, O$_3$ may show a different temporal evolution due to a variety of factors, such as local pollution, topography, influence of nearby sources or even trans-boundary transport of O$_3$ and its precursors. In addition, meteorological conditions can vary amongst different locations within large regions such as Europe, affecting O$_3$ concentrations in various ways. O$_3$ trend studies in the past have tried to tackle this issue, mainly by using clustering techniques to categorize European measurement sites based on different O$_3$ metrics (e.g. Henne et al. (2010)). For instance, a site type classification representing O$_3$ regimes between 2007 and 2010 was obtained by Lyapina et al. (2016) using mean seasonal and diurnal variations. In addition, a geographical categorization reflecting the synoptic meteorological influence on O$_3$ variation between 1998 and 2012 was obtained by Carro-Calvo et al. (2017). To tackle low spatial representation of urban and rural sites across large domains, i.e. mid-latitude North America, western Europe and East Asia, Chang et al. (2017) obtained a latitude dependent site classification with lower concentrations in western and northern Europe and higher concentrations in southern Europe. These studies indicate that the selected metric used to characterize O$_3$ in clustering leads to site classifications that represent different aspects of O$_3$ variability.

In the current study, a multidimensional clustering method that captures several influencing factors for the long-term trend of O$_3$ is presented. The temporal and spatial evolution of O$_3$ concentrations between 2000 and 2015 is studied using data provided by the European Environmental Agency (EEA). Mean O$_3$ concentrations are decomposed into the underlying frequencies based on a non-parametric time scale decomposition method to obtain the long-term (LT), seasonal (S) and short-term (W) variations. The multidimensional clustering approach is applied to the distinct frequency signals LT(t) and S(t) extracted from the observations.

In addition, long-term trends of de-seasonalized daily mean O$_3$ and meteo-adjusted peak O$_3$ concentrations are calculated. Through de-seasonalization and meteo-adjustment, a significant fraction of the meteorologically driven variability of O$_3$ is excluded from the observations, and uncertainty in the trend estimation is reduced by a large factor. Intersections of site groups, i.e. LT(t)-and S(t)-clusters, are employed to guide the study of O$_3$ long-term trends. Furthermore, changes in the amplitude and phase of the seasonal variability of O$_3$ are explored based on the S(t) signal obtained by the time scale decomposition methodology. Finally, long-term changes in the relationship between O$_3$ and temperature are estimated and discussed for the different site environments and regions in Europe.

2 Data

Data for O$_3$ surface measurements are provided by the EEA (Air Quality e-Reporting) in an hourly resolution for the period between 2000 and 2015. In this study, only time series with a maximum of 15% of missing values, and a maximum of 120 consecutive days with missing values are used for the whole period of measurements, leaving the study with 291 sites across the European domain (Fig. 1). The daily mean and the daily maximum of the 8 hour running mean based on hourly mean concentrations (MDA8 O$_3$) are calculated following the definition by the European Union Directive of 2008 (European Parliament

and Council of the European Union, 2008). For the representation of peak concentrations the following metrics are used: (a) MTDM, which is the mean of the ten highest daily maximum O_3 concentrations between May and September based on hourly mean data and (b) 4-MDA8, the mean of the four highest MDA8 O_3 concentrations per year.
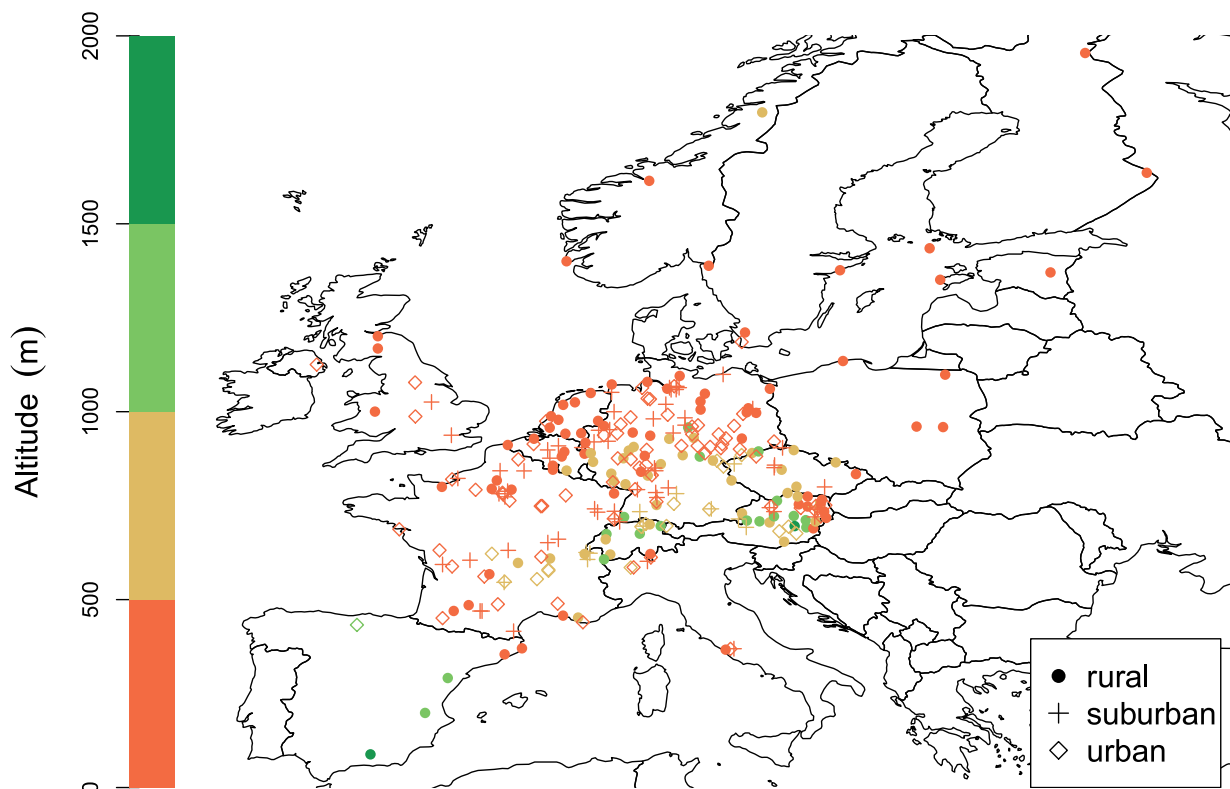
Figure 1. European map showing the location of the studied sites. Type of environment (symbols) and altitude (color bar) are indicated.

Meteorological variables are extracted from the ERA-Interim data-set on a 1 degree grid at the location (longitude-latitude-altitude) of each station and in 3-hourly intervals. The variables considered for the meteo-adjustment of the peak O_3 metrics are temperature (K), specific humidity (kg/kg^{-1}), surface pressure (hPa), boundary layer height (m), convective available potential energy (CAPE, J$\cdot$kg^{-1}), East-West surface stress (N$\cdot$s$\cdot$m^2) and North-South surface stress (N$\cdot$s$\cdot$m^2).

The present trend analysis focuses on (a) the de-seasonalized daily mean and MDA8 O_3 and (b) the meteo-adjusted MTDM and 4-MDA8 concentrations. The analysis of changes in the seasonal cycle of O_3 across Europe is based on the daily mean O_3 concentrations.

3 Methods

3.1 Time scale decomposition of daily mean and MDA8 O_3

Time scale decomposition refers to decomposition of the O_3 time series into the relevant underlying frequencies:

$$O_3(t) = LT(t) + S(t) + W(t) + E(t) \tag{1}$$

where $O_3(t)$ is the daily mean and MDA8 O_3 time series, $LT(t)$ the long-term variation, $S(t)$ the seasonal variation, $W(t)$ the short-term variation and $E(t)$ the remainder of the decomposition. Time scale decomposition in this study is performed with a non-parametric method, called the ensemble empirical mode decomposition (EEMD, Huang et al., 1998; Huang and Wu, 2008; Wu and Huang, 2009), which is considered a powerful method for decomposing O_3 time series (Boleti et al., 2018). The method detects the hidden frequencies in the time series based merely on the data and yields the so-called intrinsic mode functions (IMFs); each IMF represents one distinct frequency in the signal.

$$y(t) = \sum_{j=1}^{n} c_j(t) + LT(t) \tag{2}$$

where $y(t)$ is the input data, c_j the different IMFs, n the number of the IMFs and the remainder time series is the LT(t) of the input data. By adding together the IMFs with frequencies between around 40 days and 3 years we obtain the seasonal variation of O_3 ($S(t) = c_7(t) + ... + c_{10}(t)$) and by adding the frequencies that are smaller than 40 days the short-term variation is acquired ($W(t) = c_1(t) + ... + c_6(t)$). A more detailed discussion on the choice of the IMFs for the seasonal and short term variations can be found in the study by Boleti et al. (2018).

3.2 Cluster analysis of O_3 variations

Cluster analysis is referred to pattern recognition in high dimensional data. The main idea is to represent n objects by identifying k groups based on levels of similarity. Objects in the same group must have the highest level of similarity while objects from different groups must have low level of similarity (Jain, 2010). The partitioning around medoids (PAM) clustering algorithm is used in this study. It is based on k-means (MacQueen, 1967; Hartigan and Wong, 1979) which is a widely used clustering technique (e.g. Lyapina et al. (2016)). PAM is more robust than k-means and less sensitive to outliers, because it uses medoids (actual points in the data), instead of centroids (usually artificial points). (R Development Core Team, 2017). It works as follows: First, a set of n high dimensional objects (measurement sites) is clustered into a set of k clusters. Initially, k clusters are generated randomly and the empirical means m_k of the euclidean distance between their data points are calculated. Then, each data point is assigned to its nearest cluster center (centroid). Centroids are iteratively updated by taking the medoid of all data points assigned to their clusters. The squared error (ε) between the m_k and the points in the cluster (x_i) is calculated as:

$$\varepsilon = \sum_{i=1}^{n} \|x_i - m_k\|^2 \tag{3}$$

Each centroid defines one of the clusters and each data point is assigned to its nearest centroid, and the iterative process is terminated when the ϵ is minimized.

For identification of the clusters the LT(t), S(t) and W(t) of the daily mean and MDA8 O_3 were used as input time series in the PAM algorithm. A sufficient number of clusters must be defined in order to capture dominant behaviors such that redundant information is avoided but at the same time not overlooking important characteristics. To identify the optimal number of clusters the PAM algorithm is iteratively executed for a range of k values (number of clusters) and the average sum of ϵ (SSE) is calculated for each iteration, i.e. each k.

$$SSE = \sum_{i=1}^{n} \varepsilon^2 \qquad (4)$$

The number of clusters with the largest reduction in SSE is considered as the most representative. Eventually, the choice of the ideal number of clusters results from a combination of the SSE approach and interpretability of the obtained clusters. In addition, a Silhouette width (S_w) analysis is performed to assess the goodness of the clustering (Rousseeuw, 1987).

More details about the number of clusters, the goodness of the clustering and the S_w are provided in the supplementary material (Sections S1 and S2).

3.3 Daily mean and MDA8 O_3 long-term trend analysis

Meteorological adjustment is essential for calculation of robust O_3 long-term trends. Thus, daily mean and MDA8 O_3 observations are de-seasonalized by subtracting the S(t) obtained with the EEMD from the observations (Boleti et al., 2018)

$$y_d(t) = y(t) - S(t) \qquad (5)$$

where $y_d(t)$ is the de-seasonalized time series and $y(t)$ the observations. Through de-seasonalization observations are adjusted for the effect of meteorology on the inter-annual time scale. Theil-Sen trends (Theil, 1950; Sen, 1968) are then calculated based on monthly mean de-seasonalized concentrations $y_d(t)$ for the period 2000-2015. The 95% confidence interval of the trend is obtained by bootstrapping. The Theil-Sen trends were estimated using the *openair* library in R (R Development Core Team, 2017).

3.4 Peak O_3 concentrations long-term trend analysis

Trend analysis of peak O_3 metrics is performed for the MTDM and the 4-MDA8 O_3, based on a meteo-adjustment approach as in Boleti et al. (2019). A different approach for meteorological adjustment was used for the peak O_3 than for the daily mean and MDA8; de-seasonalization is not meaningful for peak O_3 because peak O_3 events are temporally localized. Thus, daily maximum and MDA8 O_3 observations were linked to the available meteorological variables through generalized additive models (GAMs, Hastie and Tibshirani, 1990; Wood, 2006). The models are fitted for the warm season May-September as by definition the MTDM refers to this period of the year. GAMs are instances of generalized linear models in which the model is

specified as a sum of smooth functions of the covariates. A GAM can be described as:

$$O_3(t) = \alpha + \sum_{i=1}^{n} s_i\left(M_i(t)\right) + s_0(t) + \epsilon(t) \tag{6}$$

where $O_3(t)$ stands for the O_3 time series observations (daily maximum and MDA8), α is the intercept, s_i are the smooth functions (thin plates splines) of the numeric meteorological variables M_i and n denotes the number of the numeric meteoro-
5 logical variables in the GAM. The temporal trend is represented through the smooth function $s_0(t)$, where t is the time variable expressed by the Julian day. Finally, ϵ stands for the residuals of the model. For the GAMs, the following meteorological variables were used: the daily maximum temperature, daily mean specific humidity, daily mean surface pressure, daily maximum boundary layer height, morning mean CAPE, daily mean East-West surface stress and daily mean North-South surface stress, as well as a time variable the Julian day. The above explanatory meteorological variables are the ones that were most often se-
10 lected in the Swiss sites by the meteorological variable selection performed by Boleti et al. (2019). The GAMs were estimated with the *mgcv* library in R (R Development Core Team, 2017).

The meteo-adjusted daily maximum and MDA8 O_3 concentrations were calculated similar to Barmpadimos et al. (2011) as:

$$O_{3_{metadj}}(t) = \alpha + s_0(t) + \epsilon(t) \tag{7}$$

15 where α is the intercept of the model, $s_0(t)$ the time variable as Julian day, and $\epsilon(t)$ the residuals. The meteo-adjusted MTDM and 4-MDA8 concentrations were estimated based on the meteo-adjusted values ($O_{3_{adj}}(t)$) on the same days as they were identified before the meteo-adjustment. Eventually, meteo-adjusted trends were calculated with the Theil-Sen trend estimator applied on the $O_{3_{metadj}}(t)$.

3.5 O$_3$ seasonal cycle trend analysis

20 The S(t) signal extracted with the EEMD captures the meteorologically driven O_3 variation on yearly to multi-year time scales, and is more representative compared to parametric fitting approaches (Boleti et al., 2018). Here, changes in the daily mean S(t) of O_3 throughout the studied period are identified as follows: the maximum and minimum O_3 value as well as the day when the maximum O_3 occurred in each year are identified in the S(t), referred here as S_{max}, S_{min} and S_{DoM} respectively (Fig. 2). A Theil-Sen trend estimator for each of the $S_{max}(t)$, $S_{min}(t)$ and $S_{DoM}(t)$ is applied for each site cluster, representing the
25 long-term temporal evolution of the amplitude and phase of S(t).

3.6 Relationship between O$_3$ and temperature

The relationship between O_3 and temperature is studied for the warm season May-September. A linear regression model between daily maximum O_3 concentrations and daily maximum temperature is applied for each year throughout the studied period 2000-2015 as:

30 $$O_3(t)_i = \beta_{0i} + \beta_{1i} \cdot T(t)_i, i = 1, 2, ..n \tag{8}$$
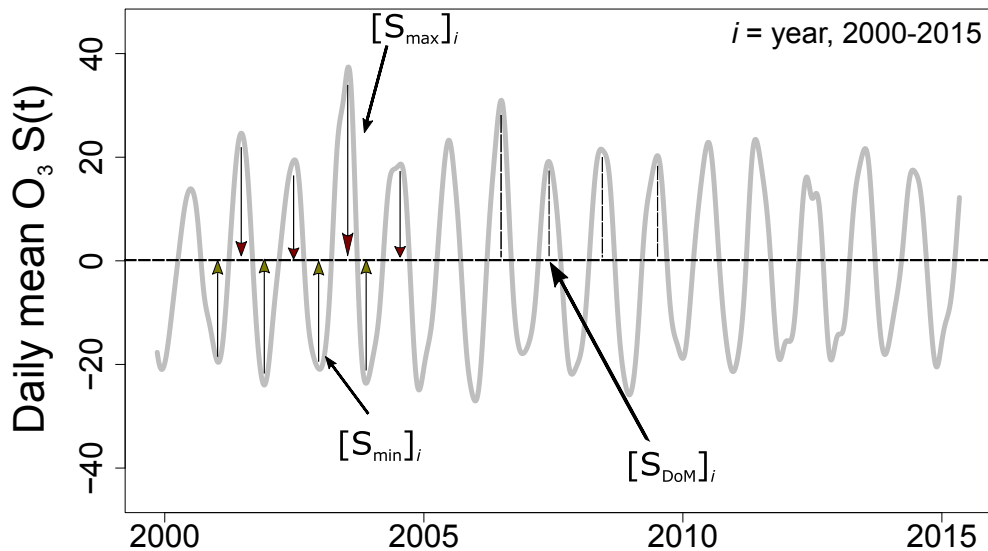
Figure 2. Schematic illustration for explaining the estimation of the ($S_{max}(t)$ and $S_{min}(t)$) and the annual day of maximum of the seasonal signal ($S_{DoM}(t)$) as calculated from the daily mean O_3 time series.

where $O_3(t)$ is the time series of the daily maximum O_3, $T(t)$ the time series of the daily maximum temperature and n is the number of years. β_{0i} is the intercept and $\beta_{1i}(t)$ the parameter describing the linear effect of temperature on O_3. Then, a linear model is applied to $\beta_{1i}(t)$ over all years for each site cluster to identify the long-term trend of the slope between O_3 and temperature maximum values. In addition, a linear regression model is applied on the daily maximum O_3 concentrations against binned temperature ranges and in three consequent time periods (2000-2005, 2005-2010 and 2010-2015).

4 Results

4.1 Cluster analysis

Here, we present the results of the daily mean LT(t)- and S(t)-clustering; results for the W(t)-clustering and the cluster analysis based on the MDA8 are provided in the supplementary material (Section S3). The clusters based on daily mean and MDA8 O_3 are rather similar, thus, the choice of clusters based on these two metrics does not affect the conclusions. The daily mean O_3 clusters depict the main influencing factors for O_3 trends, i.e. proximity to emission sources and meteorological conditions. Therefore, it is appropriate to study long-term trends based on the O_3 daily mean clusters. Application of the clustering algorithm to the LT(t) leads to a site type classification, which largely reflects the proximity to emission sources of O_3 precursors.

S(t)- and W(t)-clustering leads to a regional site classification, which reflects the importance of the climate on the annual cycle of O_3. It is observed that a few sites have a negative S_w, which means that these sites are assigned to a certain cluster although they do not really fit into any of the identified clusters (see supplementary material sections S2 an S5). Nevertheless, the sites with negative S_w were not excluded from the data analysis as they do not have a noticeable influence on the results.

5   O_3 concentrations often increase with distance from emission sources of NO_x. Thus, LT(t)-clustering leads to identification of site groups with similar type of environment in terms of proximity to precursor emissions and mean O_3 concentrations, which are indicative of multiannual changes in the O_3 time series (Boleti et al., 2018). This measurement-based classification can be more informative than reported station types, since e.g. there are rural sites with nearby pollution sources or even sites with surroundings that might have changed dramatically with time. In the following section, clusters obtained from analysis

10   of daily mean O_3 are presented and discussed in detail; the clusters derived from MDA8 O_3 are similar and presented in the supplementary material (Section S3).

Cluster analysis of the long-term variation LT(t) resulted in four clusters that mainly differ in the daily mean O_3 concentration levels: Cluster 1 includes sites that are marked in the Air Quality e-Reporting data repository as being of rural site type and sites that are mostly located at relatively high altitudes (on average 800 to 1200 m). The sites in cluster 1 show the highest

15   O_3 concentrations as illustrated in Fig. 3. The high mean O_3 concentrations indicate that the sites in cluster 1 are representing background situations with minor influence of nearby emissions of man-made O_3 precursors. This cluster is therefore denoted as background cluster ("BAC"). Cluster 2 includes mostly rural sites, that are located at lower altitudes of around 300-600 m and is therefore labelled as rural cluster ("RUR") 3. The sites in cluster 3 are also located at low altitudes (around 100 to 300 m) and represent rural, suburban and urban site types in similar numbers. The sites in cluster 3 seem to be influenced by nearby

20   man-made emissions of O_3 precursors such as NO_x, leading to lower mean O_3 concentrations compared to the sites in the "RUR" cluster. Cluster 3 consists of moderately polluted sites and denoted as cluster MOD. Finally, cluster 4 consists mostly of urban and suburban sites showing the lowest daily mean O_3 concentrations likely due to the proximity to sources of NO_x emissions and the resulting enhanced depletion of O_3 through reaction with NO. Consequently, cluster 4 is denoted as the highly polluted cluster ("HIG").

25   The LT(t) signal as derived from the daily mean (Fig. 3) and MDA8 O_3 (Fig. S9) observations increases for "BAC" and "RUR" until around beginning of 2000s and decreases afterwards. For the "MOD" and "HIG" clusters the same pattern was observed, but the decrease starts much later than in the rural sites, i.e. around end of 2000s. Especially in the "HIG" sites mostly a level-off is observed after 2010 rather than a decrease. Similar temporal evolution with inflection points in the LT(t) has been observed in the study by Boleti et al. (2018) which was focused on trends of average O_3 concentrations in Switzerland.

30   Clusters derived from the daily mean S(t) show a regional representation most likely due to the influence of the regional climate conditions an the annual cycle of O_3. The following five clusters were obtained from the daily mean S(t) (Fig. 4): (1) "CentralNorth" comprises northern and eastern part of Germany, Netherlands and some eastern sites in Czech Republic, Poland and Austria, (2) "CentralSouth" covers most part of Austria, Switzerland and some sites in the Southwest of Germany, (3) "West" incorporates the biggest part of France, Belgium and Spain, (4) "PoValley" includes the sites located in the Po

35   Valley, an industrial region in Northern Italy. (5) "North" covers most of the UK and Scandinavia. The number of sites included
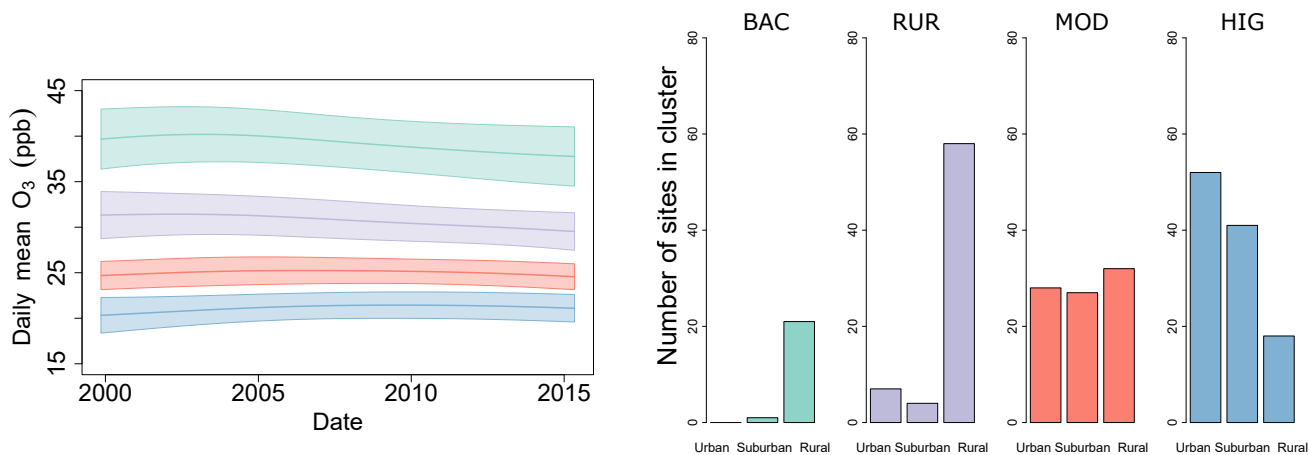
Figure 3. Clusters based on daily mean O$_3$ LT(t). Average LT(t) in each cluster with $\pm$ the standard deviation (left) and histograms for the site type included in each cluster.

in each cluster are shown in Table 1. The sites in "PoValley" display the most pronounced S(t), mainly due to the Mediterranean weather conditions, e.g. high temperatures. At the same time high NO$_x$ and VOC emissions in this region leads to higher O$_3$ concentrations. Special topographic conditions (valley south of Alps) in combination with cyclonic systems lead to containment of emissions from the Milan industrial area in Po Valley (Bärtsch-Ritter et al., 2004; Henne et al., 2005; Prévôt et al., 1997;
5   Thunis et al., 2009). The "North" cluster has the smallest seasonal variability, due to generally low O$_3$ concentrations, and lower temperature conditions in this region. Especially in the Scandinavian sites meteorological conditions are rather unfavorable for O$_3$ formation. Also, the regions included in the "North" cluster are influenced by cyclonic systems arriving in Europe through the North Atlantic ocean, that carry air pollutants into Europe (Stohl, 2002; Dentener et al., 2010). Thus, the influence of background O$_3$, i.e. O$_3$ inflow from northern America and eastern Asia, is high in these sites (Derwent et al., 2004, 2013). In
10   all clusters (except in the "North") the hot summers of 2003 and 2006 are visible in the S(t) signal, which shows that the S(t) signal can capture important events in O$_3$ variability that are driven by seasonal meteorological phenomena. It is interesting to note that both Central North sites have seasonal values in their signal comparable to the Po Valley values, probably related to industrial and agricultural emissions in the area of Northern Germany.

    A two-dimensional classification scheme is achieved by employing the LT(t)- and S(t)-clusters. Our results are in good
15   agreement with previous classification studies, where by using different O$_3$ metrics similar classifications have been obtained. For instance, the spatial analysis based on gridded O$_3$ data (MDA8) across Europe by Carro-Calvo et al. (2017) resulted in a regional site classification. The gridded data used by Carro-Calvo et al. (2017) were obtained by spatial interpolation leading to a larger and regular geographical coverage compared to the available observations. Compared to Carro-Calvo et al. (2017), similar geographical clusters were identified here, except for the Iberian Peninsula, eastern Europe, northern Scandinavia
20   and the Balkan states that do not appear as separate clusters in our analysis. This is most probably due to the small number of observational sites in the above regions. In contrast to our study, gridded MDA8 O$_3$ concentration during summer have
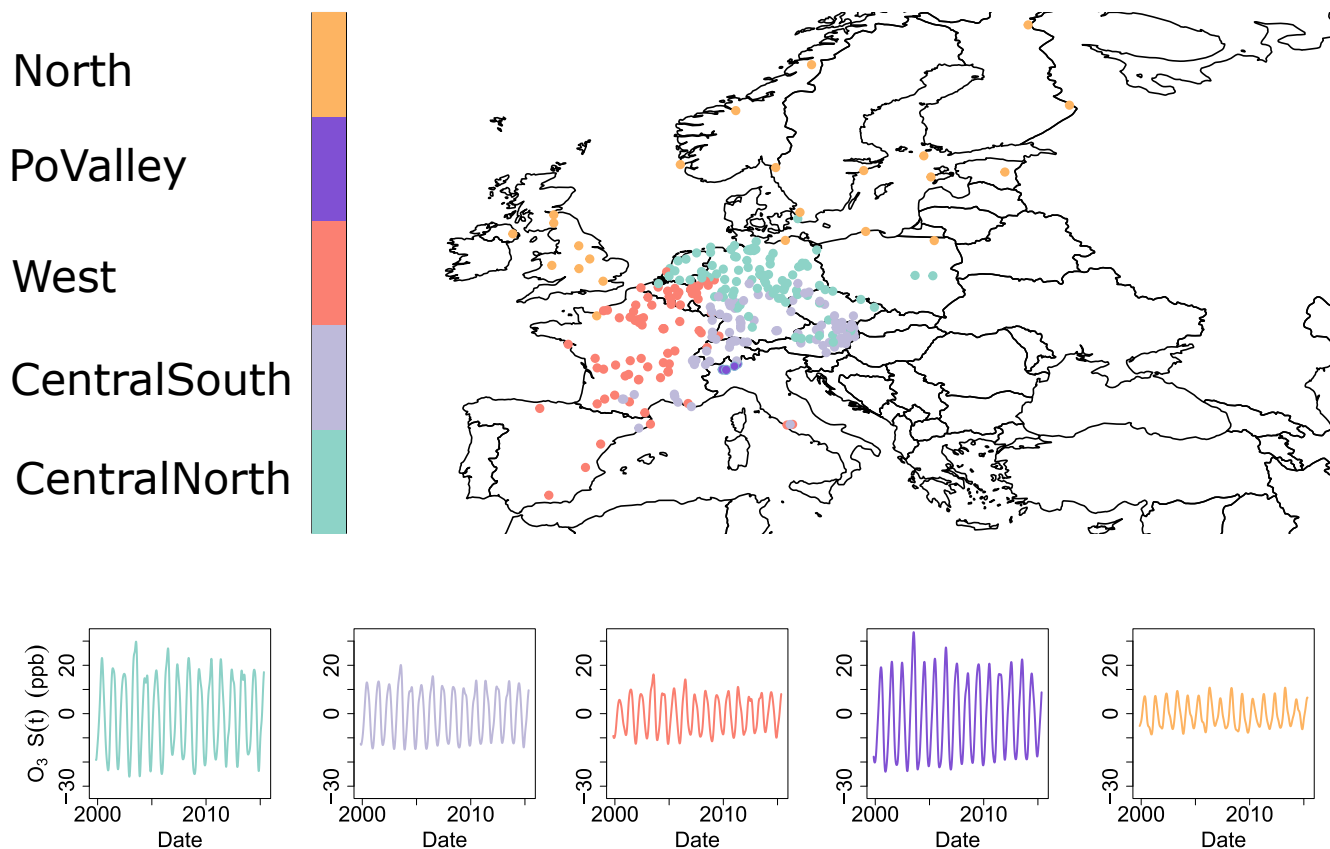
Figure 4. Map with the site clusters derived from daily O_3 S(t), and average S(t) in each site cluster.

exclusively been used for the cluster analysis by Carro-Calvo et al. (2017), therefore conditions when the correlation of O_3 and meteorological variables such as temperature is typically strongest. In addition, the present study results in spatial classification by utilizing the seasonal variation, while Carro-Calvo et al. (2017) have used normalized anomalies. Four site type clusters were found based on the LT(t) in this study similar to Lyapina et al. (2016) based on absolute mixing ratios of O_3 variations,
5   which identified five site type clusters ranging from urban traffic (as the "HIG" cluster here) to rural background environments (equivalent to "RUR"). Similar site classifications are obtained because the L(t) signal of this study and the mean seasonal and diurnal profiles of Lyapina et al. (2016) both capture the O_3 concentration levels distinguishing specific pollution regimes.

4.2 Trends of daily mean O_3 concentrations

The daily mean LT(t)- and S(t)-clusters identified in section 4.1 are used for assessment of the temporal trends for the different
10   site types and geographical locations. Overall, decreasing daily O_3 means are found for rural sites, while there is a tendency for increasing O_3 in more polluted urban environments (Fig. 5. MDA8 trends are similar to the daily mean trends, thus, are shown in

Table 1. Number of sites in each site group based on the LT(t) and S(t) clusters.

Cluster	BAC	RUR	MOD	HIG	Sum
CentralNorth	5	8	33	48	94
CentralSouth	8	29	27	28	92
West	9	16	21	31	77
PoValley	0	2	2	0	4
North	0	16	4	4	24
Sum	22	71	87	111	Total: 291

the supplementary material Section S4). In 64% of all sites significant trends (p-value<0.05) were identified for the daily mean O_3; 61% among the significant trends were negative and 39% positive. Most rural sites – "BAC" and "RUR" – experienced decreasing daily mean O_3 concentrations in all regions, as expected following the NO_x and VOC reductions in Europe (Fig. 5). At the "MOD" and "HIG" sites a levelling-off or increase is observed respectively, especially in "CentralNorth", "West" and "North" regions. At the "HIG" sites the positive trends could partly be explained by the increase of NO_2 to NO_x ratio, originating from the proliferation of diesel vehicles, that have increased in the European car fleet (EEA, 2009). In addition, the strong reduction of NO_x concentrations that led to less titration of O_3 by NO, could also explain the positive trends at urban and suburban sites. The late inflection point at urban sites (LT(t) of "HIG" cluster in Fig. 3) can be an additional effect of the reduced titration of O_3, which leads to positive trends at the "HIG" sites. Flat trends at central European sites, might partially be explained by the increasing influence of North American and Asian emissions, that have counterbalanced the decrease of European NO_x and VOC concentrations (Derwent et al., 2018; Yan et al., 2018).

In agreement with our results, significant decreases of daytime average and summertime mean of MDA8 O_3 at European rural sites as well as small and non-significant downward trends of MDA8 at urban sites have been found previously for the time period 2000-2014 (Chang et al., 2017). Similarly, in a report by EEA (2016) it was found that between 2000 and 2014 annual mean O_3 and annual mean MDA8 O_3 have been decreasing in rural background sites, while at more polluted sites influenced by nearby man-made precursor emissions, upward trends have been detected.

O_3 trends at sites in the cluster "North" indicate changes in background O_3, especially in the "RUR" ones that are mostly free from local emissions. Here, decreasing trends of daily mean O_3 were found in "RUR" sites, while in the "MOD" and "HIG" the trends are slightly increasing. It is interesting to compare the trends in the "North" cluster with the temporal evolution of O_3 in Mace Head (remote station in northwestern Ireland), which is representative for inflow of background O_3 into Europe. For this reason, we estimated the LT(t) variation of MDA8 O_3 and the Theil-Sen trend for the site in Mace Head (Fig. 6) to compare with the MDA8 O_3 trend identified by Derwent et al. (2018). Here, an inflection point was identified in the LT(t) in 2006, i.e. MDA8 O_3 has been increasing between 1988 and 2006 and started to slightly decline after 2006. De-seasonalized Theil-Sen trends were estimated 0.08 ppb/year [0.06,0.1] for the first period and -0.04 ppb/year [-0.09,0.02] for the second period.

Similarly, Derwent et al. (2018) have found an increase of 0.34 ± 0.07 ppb/year with a deceleration rate after 2007 of -0.0225 ± 0.008 ppb/year^2 at the same station, based on a combination of filtered measurement data and modeling output (Lagrangian
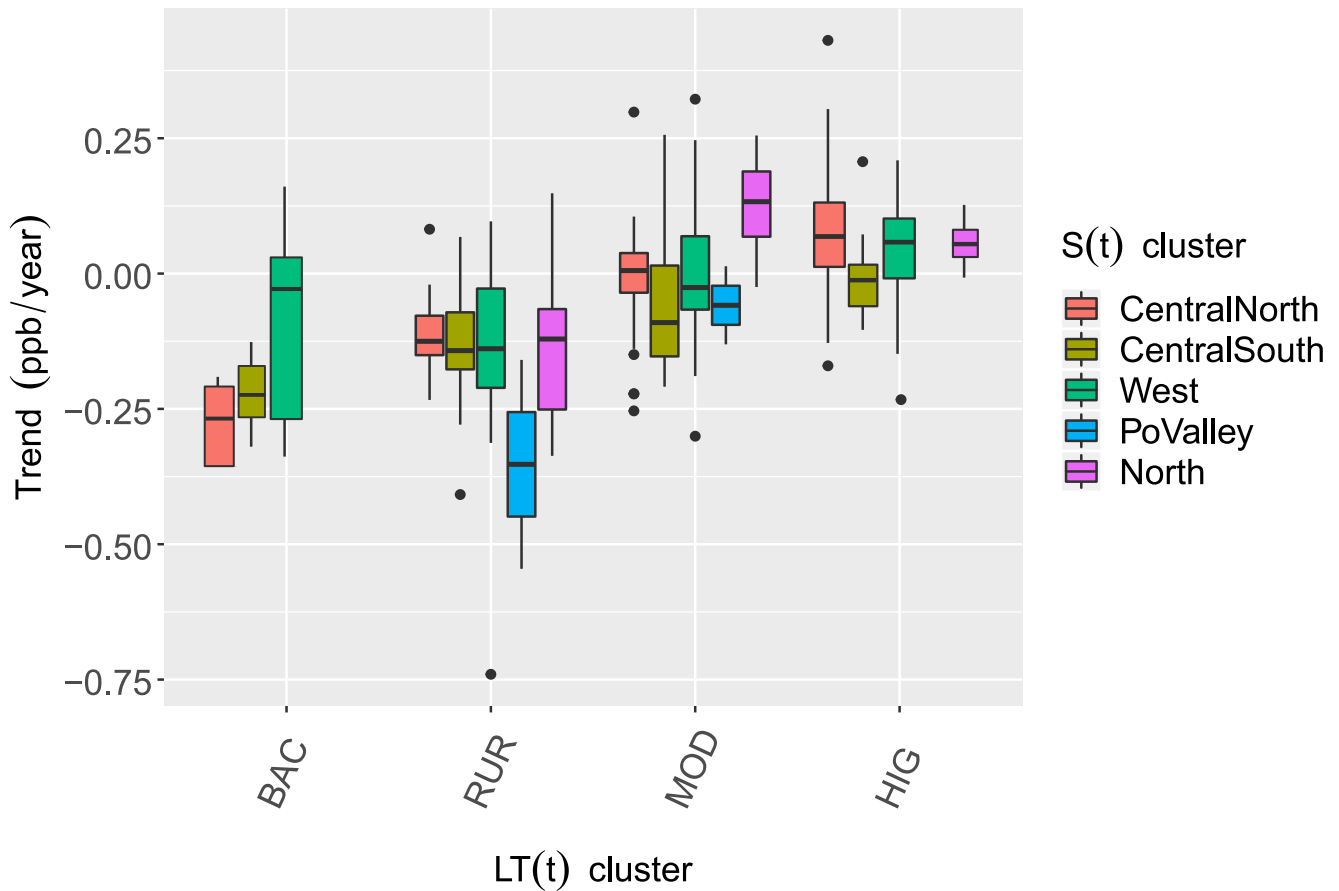
Figure 5. Box-plots of de-seasonalized daily mean O$_3$ trends for the LT(t)- and S(t)-clusters. LT(t)-clusters represent a site type classification while the S(t)-clusters a geographical one that is influenced by regional climate conditions. Boxes include 25th to 75th percentiles with the line indicating the median value; whiskers extend to 1.5 times the interquartile range.

dispersion). The inflection point in mid-2000s might be the reason for the flat trend of the annual average O$_3$ during 2000s as estimated by Derwent et al. (2013).

4.3 Trends of peak O$_3$ concentrations

Peak O$_3$ concentrations in summertime are attributed to photochemical production during this time of the year, and the spring
5   maximum in remote locations is linked to stratospheric influx as well as hemisphere-wide photochemical production during that season (Holton et al., 1995; Monks, 2000). In this study, significant negative meteo-adjusted MTDM trends were observed at 62% of the sites (ratio of sites with negative trends/number of all sites), while without meteo-adjustment significant negative
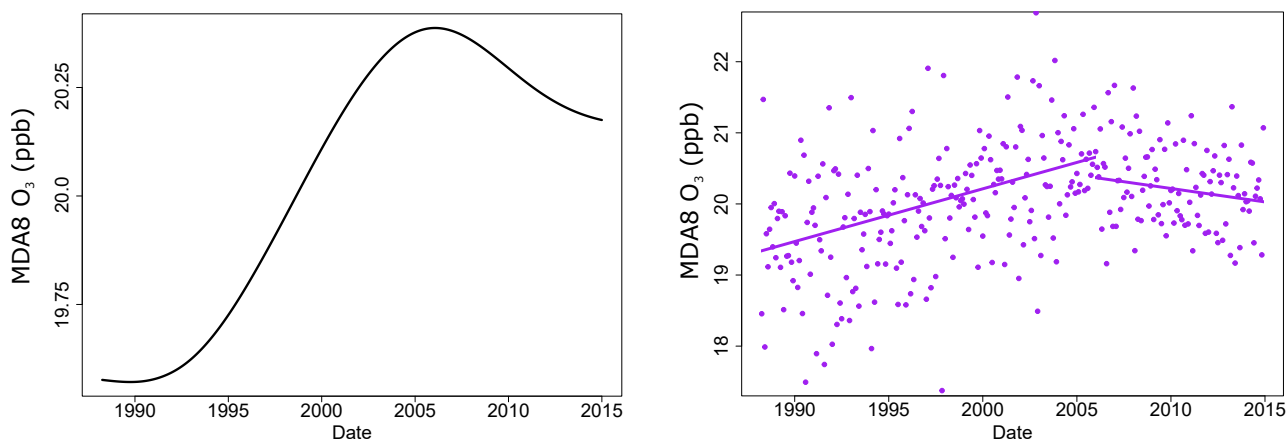
Figure 6. MDA8 LT(t) in Mace Head extracted with the EEMD (left) and the corresponding de-seasonalized Theil-Sen trend (right).

trends were identified at only 19% of the sites (4-MDA8 trends are shown in the supplementary material Section S4). The higher number of sites with significant trends after the meteo-adjustment indicates the advantage of using meteo-adjusted observations in the trend estimation. This argument is supported in the study by Fleming et al. (2018), where significant negative trends of the 4th highest MDA8 O_3 between 2000 and 2014 have been detected at only 18% of the studied sites across Europe, while at

5 a large proportion of sites either weak negative to weak positive or no trends at all were found. The non-significant trends have been attributed by Fleming et al. (2018) to the influence of meteorology which is not considered in their trend estimation.

Trends of meteo-adjusted MTDM are discussed here for the daily mean O_3 LT(t)- and S(t)-clusters. MTDM decreased for all site types and regions during the studied period 2000-2015. However, in the "RUR" cluster MTDM showed the strongest decrease among all LT(t)-clusters (Fig. 7). Interestingly, in the "BAC" cluster (especially the "West" cluster) the decrease of

10 MTDM was not so pronounced, likely due to the increase of hemispheric transport of O_3 in Europe (Derwent et al., 2007; Vingarzan, 2004). The same pattern was observed at the high alpine site of Jungfraujoch, which is representative for European continental background O_3 concentrations (Balzani-Lööv et al., 2008; Boleti et al., 2019). Also, "HIG" sites in "CentralSouth" showed slightly smaller decrease of MTDM compared to the other regions, possibly due to industrialization in the neighboring eastern Europe (Vestreng et al., 2009). Nevertheless, in order to estimate the reasons and quantify the exact influence of the

15 above factors on the trends, dedicated modelling studies are needed.

Our results are in line with a modeling sensitivity study, where negative trends of the 95th percentile of O_3 concentrations were found in European rural background sites for the period 1995-2014 (Yan et al., 2018). For the shorter time period between 1995 and 2005, downward trends of measured MTDM have been observed for most parts of Europe as well (in the range [-0.12,-0.55] ppb/year), with the highest decrease in the Czech Republic, UK and the Netherlands (on average -1 ppb/year) and

20 very small (nearly flat) in Switzerland (EEA, 2009). In our study, measured MTDM trends (2000-2015) for these regions are in the same range, i.e. the average decrease was estimated between -0.28 and -0.55 ppb/year. Smaller trends in Switzerland
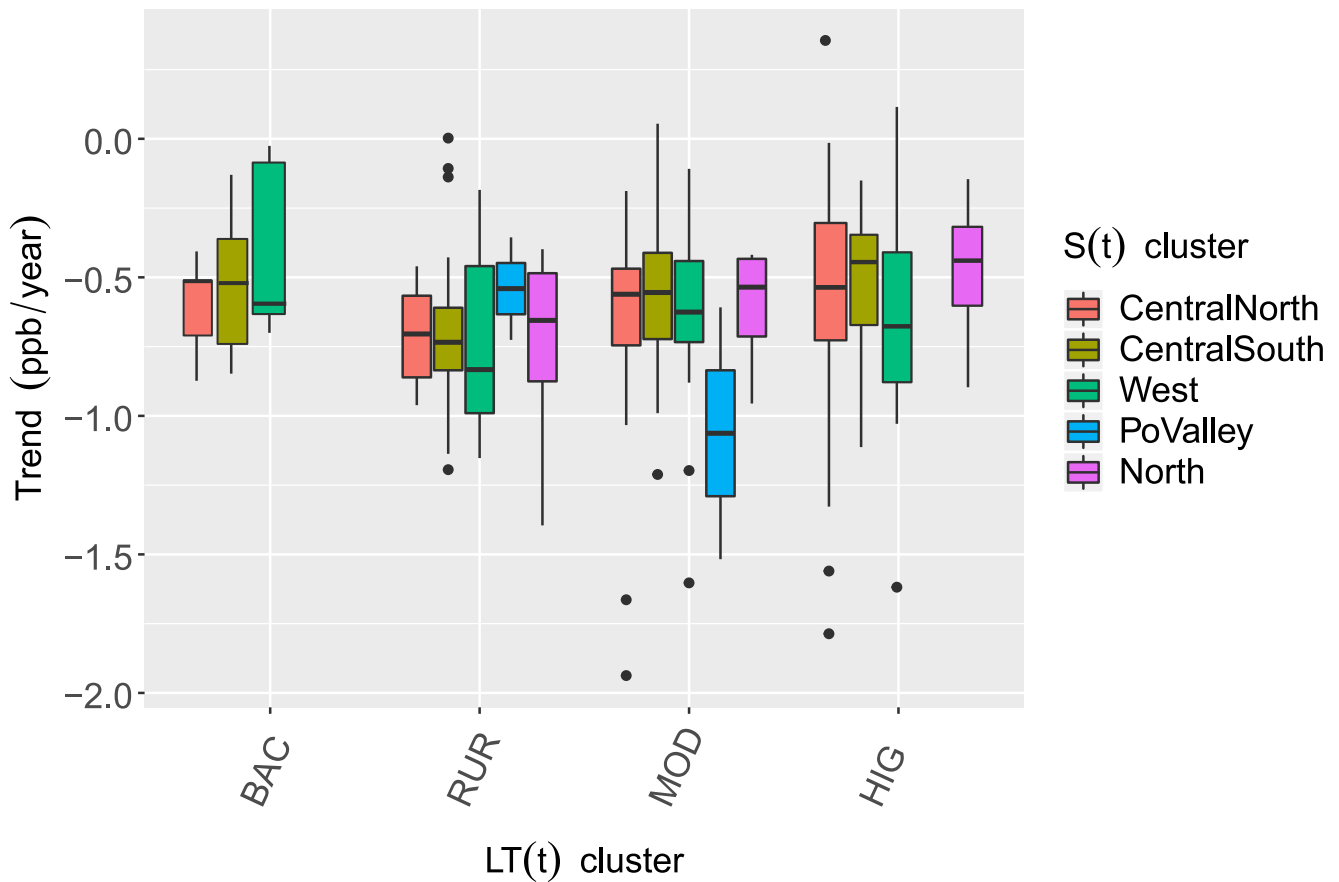
Figure 7. Box-plots of meteo-adjusted MTDM trends for the daily mean O_3 LT(t)- and S(t)-clusters. LT(t)-clusters represent a site type classification while the S(t)-clusters a geographical one that is influenced by regional climate conditions.

and central and northeast Germany have been observed by EEA (2009), which agrees with our result for the "CentralSouth" sites that showed the smallest average trend among all clusters. The flat trend in Switzerland during 1995-2005 is probably linked to the disproportional decrease of NO_x and VOCs until beginning of 2000s, when an inflection point has been observed at most polluted sites (Boleti et al., 2018). In Germany, a mixed behavior was observed by EEA (2009), with the northeastern part showing a stronger decrease and the central and northeast region a smaller decrease. Similar to our differentiation between the clusters, average MTDM trends within the "CentralNorth" cluster (with northern and northeastern Germany included) were higher and within the "CentralSouth" (covering central parts of Germany) lower.

4.4 O₃ seasonal cycle trends

Analysis of S(t) allows studying the characteristics of the annual cycle of O_3 without influence of short-term meteorological phenomena and long-term variations. Here, the trends of $S_{max}(t)$, $S_{min}(t)$ and $S_{DoM}(t)$ are presented for the five regions identified based on S(t) as calculated from daily mean O_3. In Fig. 8 the average annual O_3 cycles are shown; it is clear that in Po Valley the day of maximum O_3 occurs in summer (June-July), while in the North occurs around spring time (late March-April). This agrees with previous studies that have reported that both the highest average O_3 concentrations and extreme O_3 episodes tend to occur over the central and southern parts of Europe during summer while over northern Europe during spring (Schnell et al., 2015; Ordóñez et al., 2017). A declining amplitude of S(t) and simultaneously a phase shift towards an earlier time in the year can be observed for the 2000 to 2015 period (Table 2).

More specifically, an overall decrease in O_3 $S_{max}(t)$ by around 0.05-0.18 ppb/year and a simultaneous increase of $S_{min}(t)$ with a rate of around 0.25 ppb/year was observed for all S(t)-clusters (Fig. 9). However, in the "North" cluster the decrease of the $S_{max}(t)$ was very small and non-significant, probably due to the pronounced influence of background O_3 at these sites. The most pronounced shortening of S(t) amplitude can be seen at the "PoValley" sites, where the downward trend of peak O_3 is largest (Fig. 7). The increase in the $S_{min}(t)$ may be partially due to the decreased titration of O_3 after reductions of NO_x emissions and probably due to the increased influx of O_3 towards north and northwest Europe and more cyclonic activity in the north Atlantic during winter as well (Pausata et al., 2012). A decrease of the 95th percentile and an increase of 5th percentile of O_3 for the period 1995-2014 has been also identified in the EMEP network (rural background sites) (Yan et al., 2018). Lower summertime peaks as a result of decreased photochemical production and higher O_3 concentrations during the winter months due to decreased O_3 titration have been found in European air masses between 1987 and 2012 (Derwent et al., 2013) as well.

The trend of O_3 $S_{DoM}(t)$ is for all regions negative, i.e. the occurrence of the day of maximum O_3 has shifted to earlier days within the year with a rate of -0.47 to -1.35 days/year (Table 2, Fig. 10). The observed shift of the day of seasonal maximum might be linked to the increase of emissions in East Asia. The associated strong photochemical reaction rates, convection and NO_x sensitivity in the tropics and subtropics (Derwent et al., 2008; West et al., 2009; Fry et al., 2012; Gupta and Cicerone, 1998) have probably contributed to increased transport of air pollution to middle and northern latitudes (Zhang et al., 2016). In addition, changes in meteorological factors may have affected the seasonal variation of O_3. For instance, a similar behavior with an earlier onset of the summer date (the calendar day on which the daily circulation/temperature relationship switches sign) has been observed by Cassou and Cattiaux (2016) using observational data, while Peña-Ortiz et al. (2015) have found that summer period is extending with a rate of around 2.4 days/decade based on gridded temperature data in Europe. The positive phase of the NAO leads to increased O_3 concentrations in Europe through enhanced transport of O_3 and precursors across the North Atlantic from North America to Europe Creilson et al. (2003). An increase in baseline O_3 related to the prevailing positive NAO Index -and the associated westerly flow and intercontinental transport- during 1990s and beginning of 2000s is probably a factor contributing to the increase of the winter S_{min} O3 values (Pausata et al., 2012). The enhanced hemispheric transport of air pollutants from North America to Europe is related to increased transport through frontal systems as well (Creilson et al., 2003; Eckhardt et al., 2003). Increased O_3 in winter and spring, but not in summer, might lead to a shifting
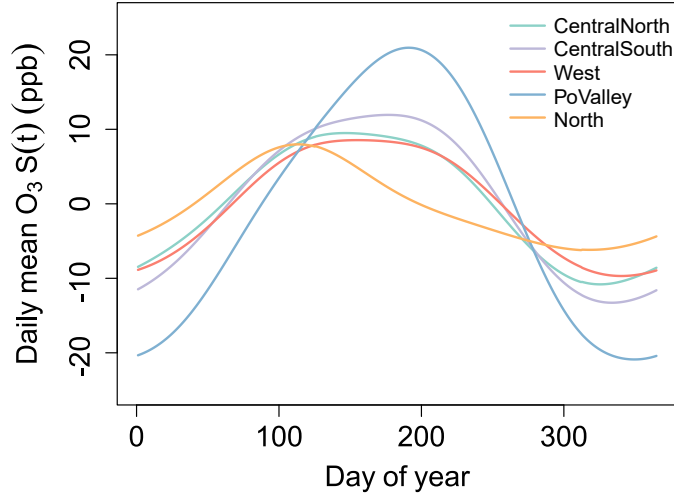
Figure 8. Annual cycle of daily mean O_3 S(t) for the daily mean S(t) clusters.

from a pronounced maximum in late summer to a broader spring-summer peak (Cooper et al., 2014). At the "West' sites a slightly stronger shift of the S_{DoMax} was observed compared to other clusters, while at the "North" sites the decrease was the smallest. The early spring maximum in the "North" sites in April (Fig. 8) can be explained by elevated NO_x that is released from PAN and alkyl nitrates that are produced during winter at northern latitudes (Brice et al., 1984; Bloomer et al., 2010).

Table 2. Linear trends of S_{max}, S_{min} and S_{DoM} for the daily mean O_3 S(t) clusters during 2000-2015. $**$ indicate highly significant trend (p-value< 0.01), $*$ significant (p-value< 0.05) and $-$ indicate non-significant trend (p-value> 0.05).

Daily mean O_3 S(t)-Cluster	Trend S_{max} (ppb/year)	Trend S_{min} (ppb/year)	Trend S_{DoM} (days/year)
CentralNorth	-0.14 ± 0.04 (**)	0.26 ± 0.03 (**)	-1.16 ± 0.18 (**)
CentralSouth	-0.17 ± 0.03 (**)	0.25 ± 0.02 (**)	-0.93 ± 0.17 (**)
West	-0.12 ± 0.04 (**)	0.26 ± 0.03 (**)	-1.35 ± 0.21 (**)
PoValley	-0.18 ± 0.6 (-)	0.30 ± 0.56 (-)	-0.65 ± 0.61 (-)
North	-0.05 ± 0.1 (-)	0.24 ± 0.07 (**)	-0.47 ± 0.38 (-)

4.5 O_3 and temperature relationship

The O_3 sensitivity to temperature is a useful metric for validation of precursor reduction scenarios and emission inventories in chemistry-transport models (Oikonomakis et al., 2018). Here, we present the long-term trends of the relationship between the daily maximum O_3 concentrations and daily maximum temperature during the warm season from May to September between
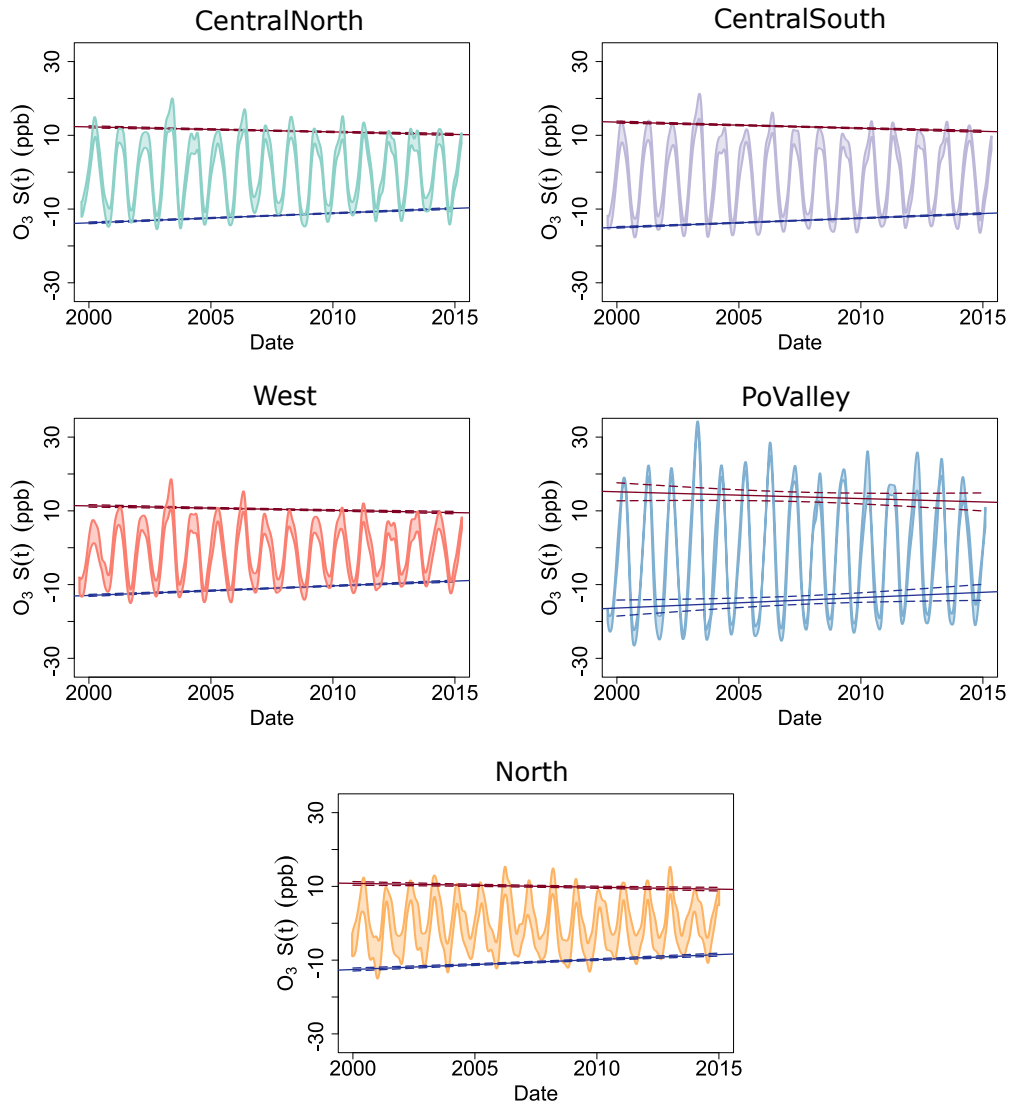
Figure 9. Temporal evolution of S_{max} and S_{min} for the daily mean O$_3$ S(t) clusters together with the average S(t) (bands indicate the average $\pm$ the standard deviation). Lines show the linear trends of S_{max} and S_{min} and dashed lines the 90% confidence interval.

2000 and 2015. Daily maximum O$_3$ and temperature are chosen in order to represent peak O$_3$ concentrations formed during the considered days.

Decreasing sensitivity of O$_3$ with respect to temperature was observed during the considered time period in all regions (Fig. 11). Fig. 11 shows the decreasing slopes of linear regression lines of maximum O$_3$ against temperature for successive year groups. The decrease is consistent for all calculated regional clusters except for "North". For most regions in Europe a significant downward trend of the slope of around 0.04-0.05 ppb/K/year was found (Table 3). At "PoValley" sites the decrease
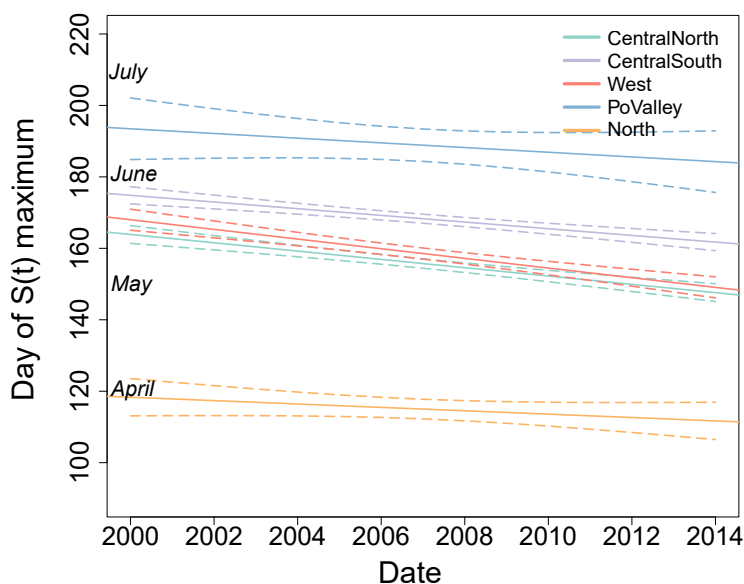
Figure 10. Linear trends of the S_{DoMax} for the daily mean S(t) clusters (dashed lines show the 90% confidence interval).

was more pronounced (-0.083 ppb/K/year) because of large reductions of precursor concentrations in this region which is characterized by high industrial emissions. Note that the average correlation between O_3 and temperature in that cluster is the highest compared to the other regions. At the "North" sites the weakest correlation of O_3 to temperature was observed and the trend is non-significant. This is expected because at these high latitudes mean temperature is lower compared to other regions

5   in Europe (Fig. 11), thus, photochemical production of O_3 is weak during the time when O_3 typically reaches its maximum concentration. In addition, in these northern regions the variability of temperature is lower compared to the central and southern parts of Europe, while O_3 concentrations are more influenced by intercontinental transport mechanisms.

     In relation to the LT(t)-clusters, it was observed that the higher the pollution burden of the site the stronger the trend of O_3 to temperature slope (Table 4). As shown here, the "HIG" and "MOD" sites have higher trends compared to the clusters "BAC"

10   and "RUR". Our results are in line with a box-model study that tested the O_3–temperature relationship under different NO_x level scenarios (Coates et al., 2016). Coates et al. (2016) have shown that at high NO_x conditions O_3 increases more strongly with temperature, while the increase is less pronounced when moving to lower NO_x conditions. Consequently, regional O_3 production has mainly decreased at the most polluted locations, due to considerable reductions of precursor emissions.

5   Conclusions

15   In this study, a classification of 291 sites across Europe was performed for the time period 2000-2015. The clustering algorithm applied on the long-term changes LT(t) and the seasonal cycle S(t) of daily mean O_3 resulted in a site type and geographical site
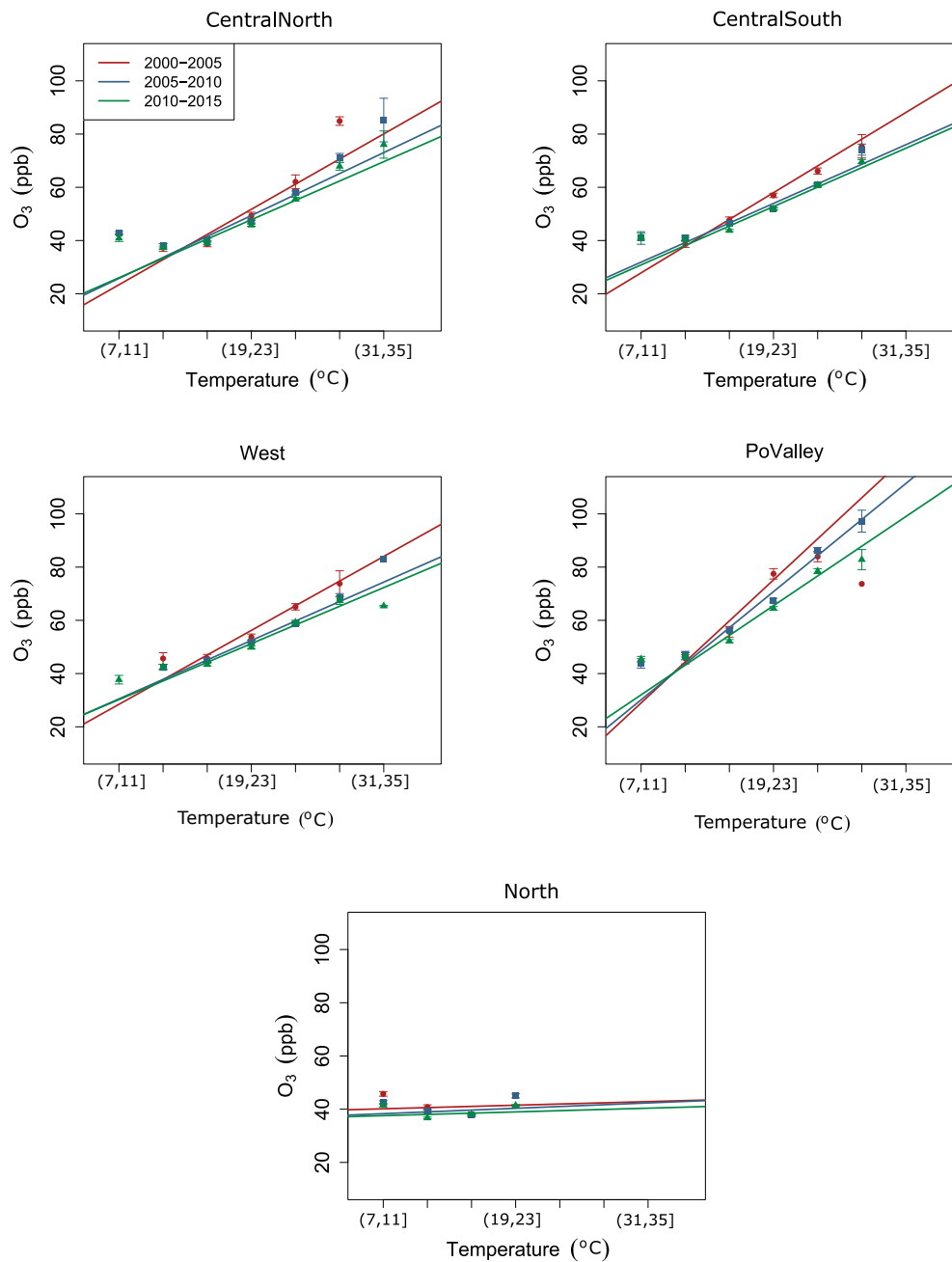
Figure 11. Linear trend of the slope between O_3-temperature daily maximum values for the warm season between May and September. The trends are calculated on the average values for each daily mean S(t) cluster and for the year groups 2000-2005, 2005-2010 and 2010-2015. Points show the mean value for the indicated temperature bin together with the corresponding standard deviation.

Table 3. Linear trends of the O_3-temperature slope (based on daily maximum values) for the daily mean O_3 S(t)-clusters for the time period 2000-2015. ∗∗ indicate highly significant trend (p-value< 0.01), ∗ significant (p-value< 0.05) and − indicate non-significant trend (p-value> 0.05).

Daily mean O_3 S(t)-Cluster	Trend (ppb/K/year)	Standard deviation	p-value
CentralNorth	-0.042	0.003	**
CentralSouth	-0.04	0.003	**
West	-0.05	0.004	**
PoValley	-0.083	0.016	**
North	-0.016	0.013	-

Table 4. Linear trends of the O_3-temperature slope (based on daily maximum values) for the daily mean O_3 LT(t)-clusters for the time period 2000-2015. ∗∗ indicate highly significant trend (p-value< 0.01), ∗ significant (p-value< 0.05) and − indicate non-significant trend (p-value> 0.05).

Daily mean O_3 LT(t)-Cluster	Trend (ppb/K/year)	Standard deviation	p-value
BAC	-0.038	0.006	**
RUR	-0.034	0.006	**
MOD	-0.043	0.003	**
HIG	-0.046	0.003	**

classification respectively. Such a two-dimensional site classification scheme provides an innovative approach for O_3 trends studies in large spatial domains and can be of significant use in model evaluation studies (e.g. Otero et al., 2018). Our approach captures several features of O_3 variations, i.e. pollution level from the L(t)-clustering and influence of the regional climate conditions from the S(t)-clustering, and presents a unifying perspective on past studies that report different site type labels based on cluster analysis using different metrics of O_3 concentrations. The two-dimensional approach offers a tool beyond traditional clustering studies to study the factors that affect O_3 trends. In addition, O_3 time series analysis is complex and benefits from being characterized in different ways, as well as grouped based on several features. The regional differentiation is hampered by sparse or missing measurement sites in some regions, e.g. eastern Europe or the Balkan peninsula. However, in the last years the number and spatial distribution of sites with longer and more dense measurements has improved.

A trend analysis of de-seasonalized mean O_3 concentrations and meteo-adjusted peak O_3 concentrations was implemented for the considered sites. By using LT(t)- and S(t)-clusters, patterns of O_3 long-term trends across Europe were investigated, based on the multi-dimensional site classification scheme. Long-term trends of de-seasonalized daily mean O_3 are decreasing at the rural sites, while in suburban and urban sites they are either stable or slightly increasing. Positive or flat trends indicate that reduction of precursors has been less effective in reducing O_3 concentrations in heavily polluted environments. On the other hand, downward trends in peak O_3 concentrations were observed in all regions, as a result of precursors emissions reductions.

However, peak O_3 has been decreasing with the smallest rate at higher altitude sites especially in the western part of Europe possibly due to the influence of background O_3 imported from North America and East Asia.

The analysis of S(t) extrema revealed a decrease in summertime maxima and an increase in wintertime minima, pointing to a decreasing amplitude of the seasonal cycle of O_3. At the same time the occurrence of the day of maximum has shifted from summer to spring months with a rate of around -0.5 to -1.3 days/year. Changes in the S(t) might be attributed on one hand to the precursors reductions in Europe, and, on the other hand, to changing weather patterns in the northern Atlantic and increase of emissions in southern East Asia.

Finally, the sensitivity of O_3 to temperature has weakened since 2000 with a rate of around 0.04 ppb/K/year, i.e. formation of O_3 became weaker at high temperature conditions, that can be attributed to the decrease of NO_x concentrations. The trend of the sensitivity differs across sites that are influenced by different meteorological conditions.

Acknowledgements. We kindly thank the Swiss Federal Office of Environment for funding this project and Dr. Stephan Henne for extracting the ERA-Interim meteorological variables.

Competing interests. The authors declare that they have no conflict of interest.

Data availability. The data used for this study can be made available upon request.

Author contributions. EB carried out the analysis. EB with CH and ST conceived the idea and methodology and wrote the manuscript. SG contributed in the data preparation and analysis. AP consulted the methodological approach and interpretation of results.

References

Anttila, P. and Tuovinen, J. P.: Trends of primary and secondary pollutant concentrations in Finland in 1994-2007, Atmospheric Environment, 44, 30–41, doi:10.1016/j.atmosenv.2009.09.041, http://dx.doi.org/10.1016/j.atmosenv.2009.09.041, 2009.

Balzani-Lööv, J. M., Henne, S., Legreid, G., Staehelin, J., Reimann, S., Prévôt, A. S. H., Steinbacher, M., and Vollmer, M. K.: Estimation of background concentrations of trace gases at the Swiss Alpine site Jungfraujoch (3580 m asl), Journal of Geophysical Research Atmospheres, 113, 1–17, doi:10.1029/2007JD009751, 2008.

Barmpadimos, I., Hueglin, C., Keller, J., Henne, S., and Prévôt, A. S. H.: Influence of meteorology on PM10 trends and variability in Switzerland from 1991 to 2008, Atmospheric Chemistry and Physics, 11, 1813–1835, doi:10.5194/acp-11-1813-2011, 2011.

Bärtsch-Ritter, N., Keller, J., Dommen, J., and Prévôt, A. S. H.: Effects of various meteorological conditions and spatial emission resolutions on the ozone concentration & ROG/NOx limitation in the Milan area (I), Atmospheric Chemistry and Physics Discussions, 3, 733–768, doi:10.5194/acp-4-423-2004, 2004.

Bloomer, B. J., Stehr, J. W., Piety, C. a., Salawitch, R. J., and Dickerson, R. R.: Observed relationships of ozone air pollution with temperature and emissions, Geophysical Research Letters, 36, 1–5, doi:10.1029/2009GL037308, 2009.

Bloomer, B. J., Vinnikov, K. Y., and Dickerson, R. R.: Changes in seasonal and diurnal cycles of ozone and temperature in the eastern U . S ., Atmospheric Environment, 44, 2543–2551, doi:10.1016/j.atmosenv.2010.04.031, http://dx.doi.org/10.1016/j.atmosenv.2010.04.031, 2010.

Boleti, E., Hueglin, C., and Takahama, S.: Ozone time scale decomposition and trend assessment from surface observations in Switzerland., Atmospheric Environment, 191, 440–451, doi:10.1016/j.atmosenv.2018.07.039, 2018.

Boleti, E., Hueglin, C., and Takahama, S.: Trends of surface maximum ozone concentrations in Switzerland based on meteorological adjustment for the period 1990-2014., Atmospheric Environment, 213, 326–336, doi:10.1016/j.atmosenv.2019.05.018, 2019.

Brice, K. A., Penkett, S. A., Atkins, D. H. F., Sandalls, F., Bamber, D., Tuck, A., and Vaughan, G.: Atmospheric measurements of peroxyacetylnitrate (PAN) in rural, south-east England: seasonal variations, winter photochemistry and long-range transport, Atmospheric Environment, 18, 2691–2702, doi:10.1016/0004-6981(84)90334-2, 1984.

Carro-Calvo, L., Ordóñez, C., García-Herrera, R., and Schnell, J. L.: Spatial clustering and meteorological drivers of summer ozone in Europe n, Atmospheric Environment, 167, 496–510, doi:10.1016/j.atmosenv.2017.08.050, 2017.

Cassou, C. and Cattiaux, J.: Disruption of the European climate seasonal clock in a warming world, Nature Climate Change, pp. 589–594, doi:10.1029/2000GL012787, https://www.nature.com/articles/nclimate2969, 2016.

Chang, K.-l., Petropavlovskikh, I., Cooper, O. R., Schultz, M. G., and Wang, T.: Regional trend analysis of surface ozone observations from monitoring networks in eastern North America, Europe and East Asia, Elementa, 5, 1–22, doi:10.1525/elementa.243, 2017.

Coates, J., Mar, K. A., Ojha, N., and Butler, T. M.: The influence of temperature on ozone production under varying NOx conditions – a modelling study, Atmospheric Chemistry and Physics, 16, 11 601–11 615, doi:10.5194/acp-16-11601-2016, https://doi.org/10.5194/acp-2017-1077, 2016.

Colette, A., Granier, C., Hodnebrog, O., Jakobs, H., Maurizi, A., Nyiri, A., Bessagnet, B., D'Angiola, A., D'Isidoro, M., Gauss, M., Meleux, F., Memmesheimer, M., Mieville, A., Roüil, L., Russo, F., Solberg, S., Stordal, F., and Tampieri, F.: Air quality trends in Europe over the past decade: A first multi-model assessment, Atmospheric Chemistry and Physics, 11, 11 657–11 678, doi:10.5194/acp-11-11657-2011, 2011.

Colette, A., Andersson, C., Baklanov, A., Bessagnet, B., Brandt, J., Christensen, J. H., Doherty, R., Engardt, M., Geels, C., Giannakopoulos, C., Hedegaard, G. B., Katragkou, E., Langner, J., Lei, H., Manders, A., Melas, D., Meleux, F., Rouïl, L., Sofiev, M., Soares, J., Stevenson, D. S., Tombrou-Tzella, M., Varotsos, K. V., and Young, P.: Is the ozone climate penalty robust in Europe?, Environmental Research Letters, 10, 084 015, doi:10.1088/1748-9326/10/8/084015, http://iopscience.iop.org/1748-9326/10/8/084015/article/, 2015.

5 Colette, A., Tognet, F., Létinois, L., Lemaire, V., Couvidat, F., Amo, R. M. A. D., Fernandez, I. A. G., Juan-aracil, I. R., Harmens, H., Andersson, C., Tsyro, S., Manders, A., and Mircea, M.: Long-term evolution of the impacts of ozone air pollution on agricultural yields in Europe A modelling analysis for the 1990-2010 period, Tech. Rep. November, European Environmental Agency, 2018.

Cooper, O. R., Parrish, D. D., Ziemke, J., Balashov, N. V., Cupeiro, M., Galbally, I. E., Gilge, S., Horowitz, L., Jensen, N. R., Lamarque, J.-F., Naik, V., Oltmans, S. J., Schwab, J., Shindell, D. T., Thompson, a. M., Thouret, V., Wang, Y., and Zbinden, R. M.:
10 Global distribution and trends of tropospheric ozone: An observation-based review, Elementa: Science of the Anthropocene, 2, 000 029, doi:10.12952/journal.elementa.000029, http://elementascience.org:80/article/info:doi/10.12952/journal.elementa.000029, 2014.

Creilson, J. K., Fishman, J., and Wozniak, a. E.: Intercontinental transport of tropospheric ozone: A study of its seasonal variability across the North Atlantic utilizing tropospheric ozone residuals and its relationship to the North Atlantic Oscillation, Atmospheric Chemistry and Physics Discussions, 3, 4431–4460, doi:10.5194/acpd-3-4431-2003, 2003.

15 Dawson, J. P., Adams, P. J., and Pandis, S. N.: Sensitivity of ozone to summertime climate in the eastern USA : A modeling case study, Atmospheric Environment, 41, 1494–1511, doi:10.1016/j.atmosenv.2006.10.033, 2007.

Dentener, F., Keating, T., and Akimoto, H.: Hemispheric Transport of Air Pollution, Part A: Ozone and Particulate Matter, Tech. Rep. 11.II.E.7, UNECE, 2010.

Derwent, R., Stevenson, D. S., Collins, W. J., and Johnson, C. E.: Intercontinental transport and the origins of the ozone observed at surface
20 sites in Europe, Atmospheric Environment, 38, 1891–1901, doi:10.1016/j.atmosenv.2004.01.008, http://linkinghub.elsevier.com/retrieve/ pii/S1352231004000603, 2004.

Derwent, R., Simmonds, P., Manning, A., and Spain, T.: Trends over a 20-year period from 1987 to 2007 in surface ozone at the atmospheric research station, Mace Head, Ireland, Atmospheric Environment, 41, 9091–9098, doi:10.1016/j.atmosenv.2007.08.008, http://linkinghub. elsevier.com/retrieve/pii/S1352231007006978, 2007.

25 Derwent, R. G., Stevenson, D. S., Doherty, R. M., Collins, W. J., Sanderson, M. G., and Johnson, C. E.: Radiative forcing from surface NOxemissions: spatial and seasonal variations, Climatic Change, 88, 385–401, doi:10.1007/s10584-007-9383-8, https://doi.org/10.1007/ s10584-007-9383-8, 2008.

Derwent, R. G., Manning, A. J., Simmonds, P. G., and Doherty, S. O.: Analysis and interpretation of 25 years of ozone observations at the Mace Head Atmospheric Research Station on the Atlantic Ocean coast of Ireland from 1987 to 2012, Atmospheric Environment, 80,
30 361–368, doi:10.1016/j.atmosenv.2013.08.003, http://dx.doi.org/10.1016/j.atmosenv.2013.08.003, 2013.

Derwent, R. G., Manning, A. J., Simmonds, P. G., and Doherty, S. O.: Long-term trends in ozone in baseline and European regionally-polluted air at Mace Head , Ireland over a 30-year period, Atmospheric Environment, 179, 279–287, doi:10.1016/j.atmosenv.2018.02.024, https://doi.org/10.1016/j.atmosenv.2018.02.024, 2018.

Eckhardt, S., Stohl, A., Beirle, S., Spichtinger, N., James, P., Forster, C., Junker, C., Wagner, T., Platt, U., and Jennings, S. G.: The North
35 Atlantic Oscillation controls air pollution transport to the Arctic, Atmospheric Chemistry and Physics, 3, 1769–1778, 2003.

EEA: Assessment of ground-level ozone in EEA member countries, with a focus on long-term trends, Tech. Rep. 7, EEA, European Environmental Agency, 2009.

EEA: Air quality in Europe — 2016 report, Tech. Rep. 28, EEA, European Environmental Agency, 2016.

EEA: Air quality in Europe — 2017 report, Tech. Rep. 13, doi:https://www.eea.europa.eu/publications/air-quality-in-europe-2017, 2017.

European Parliament and Council of the European Union: Directive 2008/50/EC of the European Parliament and of the Council of 21 May 2008 on ambient air quality and cleaner air for Europe, Tech. rep., European Parliament and Council of the European Union, doi:http://eur-lex.europa.eu/LexUriServ/LexUriServ.do?uri=OJ:L:2008:152:0001:0044:EN:PDF, 2008.

Fleming, Z. L., Doherty, R. M., Schneidemesser, E. V., Malley, C. S., Cooper, O. R., Pinto, J. P., Colette, A., Xu, X., Simpson, D., Schultz, M. G., Lefohn, A. S., Hamad, S., Moolla, R., and Solberg, S.: Tropospheric Ozone Assessment Report : Present-day ozone distribution and trends relevant to human health, Elementa: Science of the Anthropocene, 6, doi:https://doi.org/10.1525/elementa.273, 2018.

Fry, M. M., Naik, V., West, J. J., Schwarzkopf, M. D., Fiore, A. M., Collins, W. J., Dentener, F. J., Shindell, D. T., Atherton, C., Bergmann, D., Duncan, B. N., Hess, P., MacKenzie, I. A., Marmer, E., Schultz, M. G., Szopa, S., Wild, O., and Zeng, G.: The influence of ozone precursor emissions from four world regions on tropospheric composition and radiative climate forcing, J. Geophys. Res., 117, D07306, doi:10.1029/2011JD017134, 2012.

Guerreiro, C. B., Foltescu, V., and de Leeuw, F.: Air quality status and trends in Europe, Atmospheric Environment, 98, 376–384, doi:10.1016/j.atmosenv.2014.09.017, http://linkinghub.elsevier.com/retrieve/pii/S1352231014007109, 2014.

Gupta, M. L. and Cicerone, R. J.: Perturbation to global tropospheric oxidizing capacity due to latitudinal redistribution of surface sources of NOx, CH4 and CO, Geophysical Research Abstracts, 25, 3931–3934, doi:0094-8276/98/GRL- 1998900099505.00, 1998.

Hartigan, J. A. and Wong, M. A.: Algorithm AS 136: A k-means clustering algorithm, Journal of the Royal Statistical Society. Series C (Applied Statistics), 28, 100–108, 1979.

Hastie, T. and Tibshirani, R.: Generalized Additive Models, Statistical Science, 1, 297–310, doi:10.1214/ss/1177013604, http://projecteuclid.org/euclid.ss/1177013604, 1990.

Henne, S., Furger, M., and Prévôt, A. H.: Climatology of Mountain Venting–Induced Elevated Moisture Layers in the Lee of the Alps, Journal of Applied Meteorology, 44, 620–633, doi:10.1175/JAM2217.1, http://journals.ametsoc.org/doi/abs/10.1175/JAM2217.1, 2005.

Henne, S., Brunner, D., Folini, D., Solberg, S., Klausen, J., and Buchmann, B.: Assessment of parameters describing representativeness of air quality in-situ measurement sites, Atmospheric Chemistry and Physics, 10, 3561–3581, doi:10.5194/acp-10-3561-2010, https://www.atmos-chem-phys.net/10/3561/2010/, 2010.

Henschel, S., Le Tertre, A., Atkinson, R. W., Querol, X., Pandol, M., Zeka, A., Haluza, D., Analitis, A., Katsouyanni, K., Bouland, C., Pascal, M., Medina, S., and Goodman, P. G.: Trends of nitrogen oxides in ambient air in nine European cities between 1999 and 2010, Atmospheric Environment, 117, 234–241, doi:10.1016/j.atmosenv.2015.07.013, 2015.

Holton, J. R., Haynes, P. H., Mcintyre, M. E., Douglass, A. R., Rood, R. B., and Pfister, L.: Stratosphere-Troposphere exchange, Reviews of Geophysics, 33, 403–439, 1995.

Huang, N. E. and Wu, Z.: A Review on Hilbert-Huang Transform : Method and Its Applications to Geophysical Studies, Reviews of Geophysics, 46, 1–23, doi:10.1029/2007RG000228, http://rcada.ncu.edu.tw/reference010.pdf, 2008.

Huang, N. E., Shen, Z., Long, S. R., Wu, M. C., Shih, H. H., Zheng, Q., Yen, N. C., Tung, C. C., and Liu, H. H.: The empirical mode decomposition and the Hilbert spectrum for nonlinear and non-stationary time series analysis, Proceedings of the Royal Society of London. Series A: Mathematical, Physical and Engineering Sciences, 454, 903–995, doi:10.1098/rspa.1998.0193, http://dx.doi.org/10.1098/rspa.1998.0193, 1998.

IPCC: Climate Change 2013: The Physical Science Basis. Contribution of Working Group I to the Fifth Assessment Report of the Intergovernmental Panel on Climate Change, 1535 pp, 2013.

Jain, A. K.: Data clustering: 50 years beyond K-means, Pattern Recognition Letters, 31, 651–666, doi:10.1016/j.patrec.2009.09.011, http://dx.doi.org/10.1016/j.patrec.2009.09.011, 2010.

Lin, M., Horowitz, L. W., Payton, R., Fiore, A. M., and Tonnesen, G.: US surface ozone trends and extremes from 1980 to 2014: quantifying the roles of rising Asian emissions, domestic controls, wildfires, and climate., Atmospheric Chemistry & Physics, 17, 2017.

5   Lyapina, O., Schultz, M. G., and Hense, A.: Cluster analysis of European surface ozone observations for evaluation of MACC reanalysis data, Atmospheric Chemistry and Physics, 16, 6863–6881, doi:10.5194/acp-16-6863-2016, 2016.

MacQueen, J. B.: Kmeans Some Methods for classification and Analysis of Multivariate Observations, 5th Berkeley Symposium on Mathematical Statistics and Probability 1967, 1, 281–297, doi:citeulike-article-id:6083430, http://projecteuclid.org/euclid.bsmsp/1200512992, 1967.

10   Monks, P. S.: A review of the observations and origins of the spring ozone maximum, Atmospheric Environment, 34, 3545–3561, 2000.

Munir, S., Chen, H., and Ropkins, K.: Science of the Total Environment Quantifying temporal trends in ground level ozone concentration in the UK, Science of the Total Environment, 458-460, 217–227, doi:10.1016/j.scitotenv.2013.04.045, http://dx.doi.org/10.1016/j.scitotenv.2013.04.045, 2013.

Oikonomakis, E., Aksoyoglu, S., Ciarelli, G., Baltensperger, U., Prévôt, H., and Stephan, A.: Low modeled ozone production suggests

15   underestimation of precursor emissions (especially NOx) in Europe., Atmospheric Chemistry & Physics, 18, 2018.

Oltmans, S. J., Lefohn, a. S., Shadwick, D., Harris, J. M., Scheel, H. E., Galbally, I., Tarasick, D. W., Johnson, B. J., Brunke, E. G., Claude, H., Zeng, G., Nichol, S., Schmidlin, F., Davies, J., Cuevas, E., Redondas, a., Naoe, H., Nakano, T., and Kawasato, T.: Recent tropospheric ozone changes - A pattern dominated by slow or no growth, Atmospheric Environment, 67, 331–351, doi:10.1016/j.atmosenv.2012.10.057, http://dx.doi.org/10.1016/j.atmosenv.2012.10.057, 2013.

20   Ordóñez, C., Barriopedro, D., García-Herrera, R., Sousa, P. M., and Schnell, J. L.: Regional responses of surface ozone in Europe to the location of high-latitude blocks and subtropical ridges, Atmospheric Chemistry and Physics, 17, 3111–3131, doi:10.5194/acp-17-3111-2017, https://www.atmos-chem-phys.net/17/3111/2017/, 2017.

Ordóñez, C., Brunner, D., Staehelin, J., Hadjinicolaou, P., Pyle, J. A., Jonas, M., Wernli, H., and Prévot, A. S. H.: Strong influence of lowermost stratospheric ozone on lower tropospheric background ozone changes over Europe, Geophysical Research Letters, 34, 1–5,

25   doi:10.1029/2006GL029113, 2007.

Otero, N., Sillmann, J., Schnell, J. L., Rust, H. W., and Butler, T.: Synoptic and meteorological drivers of extreme ozone concentrations over Europe, Environmental Research Letters, 11, 24 005, doi:10.1088/1748-9326/11/2/024005, http://stacks.iop.org/1748-9326/11/i=2/a=024005, 2016.

Otero, N., Sillmann, J., Mar, K. A., Rust, H. W., Solberg, S., Andersson, C., Engardt, M., Bergström, R., Bessagnet, B., Colette, A., Couvidat,

30   F., Cuvelier, C., Tsyro, S., Fagerli, H., Schaap, M., Manders, A., Mircea, M., Briganti, G., Cappelletti, A., Adani, M., D'Isidoro, M., Pay, M.-T., Theobald, M., Vivanco, M. G., Wind, P., Ojha, N., Raffort, V., and Butler, T.: A multi-model comparison of meteorological drivers of surface ozone over Europe, Atmospheric Chemistry and Physics, 18, 12 269–12 288, doi:10.5194/acp-18-12269-2018, https://www.atmos-chem-phys.net/18/12269/2018/, 2018.

Paoletti, E., De Marco, A., Beddows, D. C. S., Harrison, R. M., and Manning, W. J.: Ozone levels in European and USA cities are increasing

35   more than at rural sites, while peak values are decreasing, Environmental Pollution, 192, 295–299, doi:10.1016/j.envpol.2014.04.040, http://dx.doi.org/10.1016/j.envpol.2014.04.040, 2014.

Parrish, D. D., Law, K. S., Staehelin, J., Derwent, R., Cooper, O. R., Tanimoto, H., Volz-Thomas, a., Gilge, S., Scheel, H. E., Steinbacher, M., and Chan, E.: Lower tropospheric ozone at northern midlatitudes: Changing seasonal cycle, Geophysical Research Letters, 40, 1631–1636, doi:10.1002/grl.50303, 2013.

Pausata, F. S. R., Pozzoli, L., Vignati, E., and Dentener, F. J.: North Atlantic Oscillation and tropospheric ozone variability in Europe : model
5   analysis and measurements intercomparison, Atmospheric Chemistry and Physics, 12, 6357–6376, doi:10.5194/acp-12-6357-2012, 2012.

Peña-Ortiz, C., Barriopedro, D., and García-Herrera, R.: Multidecadal Variability of the Summer Length in Europe, Journal of Climate, 28, 5375–5388, doi:10.1175/JCLI-D-14-00429.1, https://doi.org/10.1175/JCLI-D-14-00429.1, 2015.

Prévôt, A. S. H., Staehelin, J., Kok, L., Schillawski, D., Neininger, B., Staffelbach, T., Neftel, A., Wernli, H., and Dommen, J.: The Milan photooxidant plume, Journal of Geophysical Research, 102, 23 375–23 388, doi:10.1029/97JD01562, 1997.

10   Querol, X., Alastuey, A., Reche, C., Orio, A., Pallares, M., Reina, F., Dieguez, J. J., Mantilla, E., Escudero, M., Alonso, L., Gangoiti, G., and Millán, M.: On the origin of the highest ozone episodes in Spain, Science of the Total Environment, 572, 379–389, doi:10.1016/j.scitotenv.2016.07.193, http://dx.doi.org/10.1016/j.scitotenv.2016.07.193, 2016.

R Development Core Team: R: A Language and Environment for Statistical Computing, R Foundation for Statistical Computing, Vienna, Austria, http://www.R-project.org, ISBN 3-900051-07-0, 2017.

15   Rousseeuw, P. J.: Silhouettes : a graphical aid to the interpretation and validation of cluster analysis, Journal of Computational and Applied Mathematics, 20, 53–65, doi:10.1016/0377-0427(87)90125-7, 1987.

Schnell, J. L., Prather, M. J., Josse, B., Naik, V., Horowitz, L. W., Cameron-Smith, P., Bergmann, D., Zeng, G., Plummer, D. A., Sudo, K., Nagashima, T., Shindell, D. T., Faluvegi, G., and Strode, S. A.: Use of North American and European air quality networks to evaluate global chemistry–climate modeling of surface ozone, Atmospheric Chemistry and Physics, 15, 10 581–10 596, doi:10.5194/acp-15-
20   10581-2015, https://www.atmos-chem-phys.net/15/10581/2015/, 2015.

Sen, P.: Estimates of the regression coefficient based on Kendall's tau, Journal of American Statistical Association, 63, 1379–1389, doi:10.1080/01621459.1968.10480934, 1968.

Sillman, S. and Samson, P. J.: Impact of temperature on oxidant photochemistry in urban, polluted rural and remote environments, Journal of Geophysical Research-Atmospheres, 100, 11 497–11 508, doi:10.1029/94JD02146, 1995.

25   Simon, H., Reff, A., Wells, B., Xing, J., and Frank, N.: Ozone trends across the United States over a period of decreasing NOx and VOC emissions, Environmental Science and Technology, 49, 186–195, doi:10.1021/es504514z, 2015.

Stohl, A.: On the pathways and timescales of intercontinental air pollution transport, Journal of Geophysical Research, 107, 1–17, doi:10.1029/2001JD001396, 2002.

Theil, H.: A rank-invariant method of linear and polynomial regression analysis, Part 3, in: Proceedings of Koninalijke Nederlandse Akademie
30   van Weinenschatpen A, vol. 53, pp. 1397–1412, doi:10.1007/978-94-011-2546-8_20, 1950.

Thunis, P., Triacchini, G., White, L., Maffeis, G., and Volta, M.: Air pollution and emission reductions over the Po-valley: Air Quality Modelling and Integrated Assessment, pp. 13–17, 2009.

Vestreng, V., Ntziachristos, L., Semb, A., Reis, S., Isaksen, I. S. A., and Tarras, L.: Evolution of NO x emissions in Europe with focus on road transport control measures, Atmospheric Chemistry and Physics, 9, 1503–1520, www.atmos-chem-phys.net/9/1503/2009/, 2009.

35   Vingarzan, R.: A review of surface ozone background levels and trends, Atmospheric Environment, 38, 3431–3442, doi:10.1016/j.atmosenv.2004.03.030, 2004.

West, J. J., Naik, V., Horowitz, L. W., and Fiore, A. M.: Effect of regional precursor emission controls on long-range ozone transport – Part 1: Short-term changes in ozone air quality, Atmospheric Chemistry and Physics, 9, 6077–6093, doi:10.5194/acp-9-6077-2009, https://www.atmos-chem-phys.net/9/6077/2009/, 2009.

Wild, O. and Akimoto, H.: Intercontinental transport of ozone and its precursors in a three-dimensional global CTM, Journal of Geophysical Research: Atmospheres, 106, 27 729–27 744, 2001.

Wood, S.: Generalized Additive Models: An Introduction with R., Chapman & Hall/CRC press, 2006.

Wu, Z. and Huang, N. E.: Ensemble Empirical Mode Decomposition: A noise-assisted data analysis method, Advances in Adaptive Data Analysis, 1, 1–41, doi:10.1142/S1793536909000047, 2009.

Yan, Y., Pozzer, A., Ojha, N., Lin, J., and Lelieveld, J.: Analysis of European ozone trends in the period 1995-2014, Atmospheric Chemistry and Physics, doi:10.5194/acp-18-5589-2018, 2018.

Zhang, Y., Cooper, O. R., Gaudel, A., Thompson, A. M., Nédélec, P., Ogino, S.-Y., and West, J. J.: Tropospheric ozone change from 1980 to 2010 dominated by equatorward redistribution of emissions, Nature Geoscience, 1, doi:10.1038/ngeo2827, http://www.nature.com/doifinder/10.1038/ngeo2827, 2016.